IEEE Access
Multidisciplinary ⋮ Rapid Review ⋮ Open Access Journal

Received 11 October 2022, accepted 20 December 2022, date of publication 23 December 2022,
date of current version 30 December 2022.

Digital Object Identifier 10.1109/ACCESS.2022.3231990

RESEARCH ARTICLE

Optimal Base Placement of a 6-DOFs Robot to Cover Essential Activities of Daily Living

JAVIER DARIO SANJUAN DE CARO[1,2], MD. SAMIUL HAQUE SUNNY[3], ELIAS JOSE MUÑOZ MONTENEGRO[1], HELAL UDDIN AHMED[4], AND MOHAMMAD H. RAHMAN[1,4], (Senior Member, IEEE)

[1]Department of Mechanical Engineering, University of Wisconsin–Milwaukee, Milwaukee, WI 53212, USA
[2]Department of Mechanical Engineering, Universidad del Norte, Barranquilla 081007, Colombia
[3]Department of Computer Science, University of Wisconsin–Milwaukee, Milwaukee, WI 53212, USA
[4]Biorobotics Laboratory, University of Wisconsin–Milwaukee, Milwaukee, WI 53212, USA

Corresponding author: Javier Dario Sanjuan De Caro (jdecaro@uninorte.edu.co)

This work was supported in part by the National Institute on Disability, Independent Living, and Rehabilitation Research (NIDILRR) under Grant 90DPGE0018-01-00; and in part by the NIDILRR Center within the Administration for Community Living (ACL), Department of Health and Human Services (HHS).

ABSTRACT The number of individuals with upper or lower extremities dysfunction (ULED) has considerably increased in the past decades resulting in a high economic burden for the families and society. Individuals with ULEDs require assistive robots to fulfill all their activities of daily living (ADLs). Thus, this research presents an objective function for base placement optimization of assistive robots to increase the workspace required to fulfill ADLs (workspace coverage). The workspace coverage was determined using the xArm 6 robot and experimenting with different ADLs. Also, an object collision algorithm is implemented to avoid collisions between the robot and the user within the workspace. Moreover, the algorithm determines the existence of singularities within the workspace by computing the manipulability index. However, since the manipulability index computation depends on the Jacobian matrix's eigenvalues yielding incongruences in the units, we divided the Jacobian matrix into two parts; one for the angular and another for the linear velocity. Finally, using the objective function with a genetic algorithm (GA), the optimal base placement for the robot is obtained and validated experimentally.

INDEX TERMS Robot optimization, base placement optimization, inverse kinematics, object collision application.

NOMENCLATURE

DOF	Degree of Freedom
ULED	Upper or lower extremities dysfunction
SCI	Spinal cord injury
ALS	Amyotrophic lateral sclerosis
CVA	Cerebral vascular accident
DH	Denavit-Hartenberg
HTM	Homogeneous transformation matrix
GA	Genetic algorithm
MPSO	Particle swarm optimization
OBB	Oriented bounded box

The associate editor coordinating the review of this manuscript and approving it for publication was Jingang Jiang.

I. INTRODUCTION

The quality of life of an individual relies on the proper functioning of their extremities because most of the activities of daily living (ADL) depend either fully or partially on the extremities. However, through the decades, the wide variety of people with Upper or Lower Extremities dysfunction (ULED) has been growing at an alarming pace. Approximately 1.7% of the United States population, or 5.35 million US human beings, dwell with a central nervous system disorder that yields ULED [1]. The main reasons for ULED are spinal cord injury (SCI), amyotrophic lateral sclerosis (ALS), Cerebral Vascular Accident (CVA), trauma, amputee, and occupational injuries. From those illnesses, 353.000 Americans suffer from SCI (with 17.500 new instances each year), and greater than 795.000 US human beings go through a CVA every year [1]. Estimation indicates that forty-one million custodians deliver 34 billion hours of care yearly, resulting in excessive expenses for the households of people with ULED [2]. Thus, the help of most people enduring long-time disabilities ends in extreme social and financial impacts.

Patients with ULED require the use of a wheelchair. Only in the USA, about 3.6 million people use a wheelchair [2]. The populace of wheelchair customers doubled in the decade, with an annual growth of 5.9% [2], [3], [4], [5]. Furthermore, of the population of wheelchair users, only 10% document that they succeed in performing all their ADLs [6]. Assistive robots have shown immense potential to increase the independence of wheelchair users or individuals with ULED. For example, Obi is a feeding assistance robot that helps individuals with ULED to eat [7]. Other examples include more capabilities, as is the case of the JACO arm and the EDAN robot [8], [9], which are usually attached to the wheelchair and are capable of feeding and handling diverse objects, increasing the independence of ULED individuals. Installing a robotic device in a wheelchair requires a complete identification of the user's needs and the specific ADL. However, a method for the workspace identification of specific ADLs of an assistive robot is not available. Thus, researchers of assistive robots use their expertise to decide the proper robot placement.

The optimal robot placement is of fundamental importance for securing the maximum functionality in terms of performance [10], [11]. However, in the case of assistance robots, this problem is not straightforward because such robots do not follow a specific trajectory but consider a workspace for each ADL. For example, just by picking a mug from a table, the object's set of orientations and the table's different sizes create a whole workspace that the robot needs to fulfill. Moreover, the robot placement needs to guarantee no singular configurations within the workspace, and no collision between the robot and the user [12].

The subject of robot placement has been of interest to researchers, resulting in multiple methods to find the optimal base placement. An approach to maximize the reachability of robotic manipulators using a cost function that propels the workspace envelope in terms of surface patches towards the target points subject to functionality constraints presented in [13]. Similarly, Janardhanan et al. presented an optimization methodology for robot placement that minimizes cycle time, improving the robot performance [14]. Analogously, Yang et al. reported a strategy for the optimal placement for minimum time coordinated motion by considering the slowest axis and using the steepest-descend algorithm [15]. Complementary papers use multiple performance indices to find the optimal robot placement, with the most common strategies using the manipulability index [16], velocity performance index [17], [18], and a combination of multiple indices as is the case of Zeghloul and Pamanes-Garcia [19], Pamenas and Zeghloul [20], and Pamanes et al. [21]. However, none of those methods consider the collisions of objects as criteria for robot placement. Thus, other methodologies apply object collision algorithms as presented by Ur-Rehman et al. [22], Spensieri et al. [23], and Doan et al. [12]. Nonetheless, the algorithms presented in those researches suffer from considerable simplifications that are too conservative, e.g., considering the links as a sphere [24]. The previous approaches have been used mainly in industrial applications where the end-effector follows a predefined trajectory or a path. However, the problem of object placement for multiple workspaces has not been addressed to the extent of our knowledge. This article presents an objective function for finding the optimal placement for a set of workspaces of a 6-DOFs assistive robot. Each workspace represents a different ADL, which, when merged, yields the overall workspace of the assistive robot. The objective function integrates both collisions and singularity constraints. One novelty is using an oriented bounding box (OBB) to represent each robot link instead of spheres. OBB yields a less conservative illustration of objects in space, as it has up to six DOFs to describe the shape and orientation of a link [25]. Similar to the approaches found in the literature, the objective function uses the determinant of the Jacobian matrix to find singularities. However, instead of considering a single Jacobian matrix, we separated the Jacobian matrix to consider the orientation and position singularities separate. This approach softens the analysis of some sections of the workspace because, for some ADLs, the robot requires to reach a given location with a minimal orientation capability. The resultant objective function is continuous because we consider the complete workspace generated by each base placement. The objective function is optimized using genetic algorithms (GA) [26], [27], [28], [29] obtaining a workspace coverage that is almost three times bigger at the initial position.

TABLE 1. DH parameters of the xArm-6 robot.

	a_{i-1}	α_{i-1}	d_i	θ_i
Joint 1	0	0	L_1	θ_1
Joint 2	0	$-\frac{\pi}{2}$	0	$\theta_2 +^0 \theta_2$
Joint 3	L_2	0	0	$\theta_3 +^0 \theta_3$
Joint 4	L_3	$-\frac{\pi}{2}$	L_4	θ_4
Joint 5	0	$\frac{\pi}{2}$	0	θ_5
Joint 6	L_5	$-\frac{\pi}{2}$	L_6	θ_6

This research is organized as follows: section II presents preliminary considerations to implement the objective function, i.e., robot kinematics, the definition of the workspace for each ADL, the singularity algorithm, and the collision algorithm. Section III presents the objective function and the optimization algorithm. Then, section IV shows the results and validation of the optimization. Finally, section V presents the conclusions.

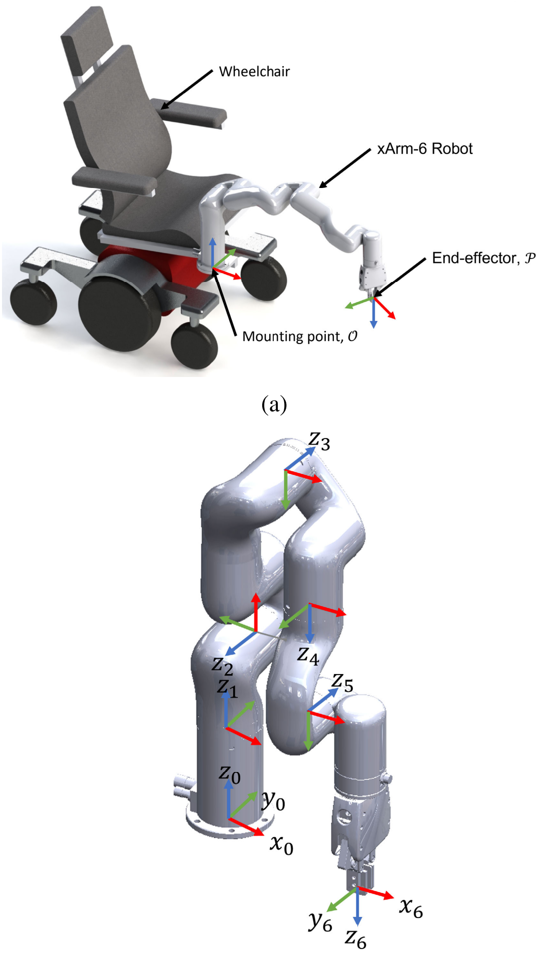

(a)

(b)

FIGURE 1. Wheelchair-mounted xArm-6 robot.

II. PRELIMINARIES

A. ASSISTIVE ROBOT

In this research, the xArm-6 mounted in a wheelchair is considered to provide ADL assistance to individuals with ULED. The xArm 6 is a serial robot of 6 DOF with six revolute joints. The Denavit Hartenberg (DH) parameters corresponding to the robot configuration shown in Fig. 1b are presented in Table-1, with the homogeneous transformation matrix (HTM) [30] derived from the DH parameters is expressed as follows:

$$
{}^{i-1}T_i = \begin{bmatrix} 1 & 0 & 0 & a_{i-i} \\ 0 & c\alpha_{i-i} & -s\alpha_{i-i} & 0 \\ 0 & s\alpha_{i-i} & c\alpha_{i-i} & 0 \\ 0 & 0 & 0 & 1 \end{bmatrix} \begin{bmatrix} c\theta_i & -s\theta_i & 0 & 0 \\ s\theta_i & c\theta_i & 0 & 0 \\ 0 & 0 & 1 & d_i \\ 0 & 0 & 0 & 1 \end{bmatrix}
$$

$$
\begin{aligned}
\alpha_{i-1} &= \text{link twist} \\
a_{i-1} &= \text{link length} \\
\theta_i &= \text{joint variable of revolute joint} \\
d_i &= \text{link offset and/or joint variable of prismatic joint} \\
c &= \cos \\
s &= \sin
\end{aligned}
\tag{1}
$$

As shown in Fig. 1a, the base frame $\mathcal{O}$ of the robot is located at the point O, at the mounting plate of the robot.

1) DIRECT KINEMATICS

The HTM yields the position and orientation (pose) of the end-effector, as given in the following equation:

$$
{}^0T_6 = \begin{bmatrix} & {}^0R_6 & & {}^0P_6 \\ 0 & 0 & 0 & 1 \end{bmatrix} \tag{2}
$$

where the column vector ${}^0P_6$ represents the position of the end-effector, while the rotation matrix ${}^0R_6$ represents the orientation of the end-effector. The components of each sub-matrix are as follows:

$$
{}^0R_6 = \begin{bmatrix} c\theta_y c\theta_z & s\theta_y s\theta_x c\theta_z - c\theta_x s\theta_z & s\theta_x s\theta_z + c\theta_x s\theta_y c\theta_z \\ c\theta_y s\theta_z & -s\theta_y s\theta_x s\theta_z + c\theta_x c\theta_z & -s\theta_x c\theta_z + c\theta_x s\theta_y s\theta_z \\ -s\theta_y & c\theta_y s\theta_x & c\theta_y c\theta_x \end{bmatrix} \tag{3}
$$

$$
{}^0P_6 = \begin{bmatrix} x \\ y \\ z \end{bmatrix} \tag{4}
$$

where θ_x is the roll angle, θ_y is the pitch angle, and θ_z is the yaw angle of the Euler angles.

The successive multiplication of the HTM of each joint yields the pose of the end effector:

$$
{}^0T_1\,{}^1T_2\,{}^2T_3\,{}^3T_4\,{}^4T_5\,{}^5T_6 = {}^0T_6 \tag{5}
$$

Thus, HTM ${}^0T_6$ represents the direct kinematics of the end-effector.

2) INVERSE KINEMATICS

Inverse kinematics is the computation of the joint positions given the end-effector pose by solving a non-linear set of transcendental equations. The literature presents multiple methods to find the inverse kinematic problem, including algebraic methods [31], [32], geometrical approaches [33], [34], [35], the Buchberger's algorithm [36], among others. Although the analytical methods can theoretically yield a proper solution for the inverse kinematic problem, in some cases, the amount of symbolic computation required makes them infeasible; this is the case of the xArm 6 robot, which analytical solution is not available. Thus, this research implements a numerical algorithm for finding the inverse kinematics based on the modified Powell's method. The modified Powell method has advantages over other numerical methods because it computes the jacobian matrix numerically using Broyden's method [37], avoiding singular solutions [38] or high iterations to converge [39]. However, Powell's method does not use box constraints to bound the inverse kinematics solution; thus, we include an additional step of joint projections to incorporate joint restrictions.

Algorithm 1 Joint Projection Algorithm

```
procedure Projection($\theta$, $\underline{\theta}$, $\overline{\theta}$)
    for $i$ in $\theta$ do
        while $\theta_i < \underline{\theta_i}$ or$\theta_i > \overline{\theta_i}$ do
            if $\theta_i < \underline{\theta_i}$ then
                $\theta_i \leftarrow \underline{\theta_i} - (\theta_i - \underline{\theta_i})$
            end if
            if $\theta_i > \overline{\theta_i}$ then
                $\theta_i \leftarrow \overline{\theta_i} - (\theta_i - \overline{\theta_i})$
            end if
        end while
    end for
    return $\theta$
end procedure
```

Let obtain the pose of the robot from equation (5) using a function $f(\theta) = Pose\left({}^{0}T_6\right)$, were:

$$\theta = \begin{bmatrix}\theta_1 & \theta_2 & \theta_3 & \theta_4 & \theta_5 & \theta_6\end{bmatrix} \tag{6}$$

Then, given the desired goal pose $g \in \mathcal{R}^6$:

$$g = \begin{bmatrix}\theta_x & \theta_y & \theta_z & x & y & z\end{bmatrix} \tag{7}$$

We seek to find the joint angles θ^* that minimizes the difference between the goal pose and the end-effector pose:

$$\begin{aligned}\theta^* &= \min_{\theta} \frac{1}{2}||g - f(\theta)|| \\ &= \min_{\theta} \mathcal{G}(\theta)\end{aligned} \tag{8}$$

Equation (8) defines the inverse kinematics objective function $\mathcal{G}(\theta)$ with joint limits implemented using box constraints:

$$\begin{aligned}\theta^* &= \min_{\theta} \mathcal{G}(\theta) \\ &\underline{\theta_i} \le \theta_i \le \overline{\theta_i}\end{aligned} \tag{9}$$

The values of $\underline{\theta_i}$ and $\overline{\theta_i}$ for each joint are presented in table (2). Thus, equation (8) is solved numerically using the modified Powell's method, using the MINPACK library [40]. However, Powell's method does not use box constraints to bound the inverse kinematics solution; thus, we include an additional step of joint projections to incorporate joint restrictions. Thus, the constraints are incorporated using the joint projection algorithm presented in the algorithm1. The joint projection algorithm runs at every iteration of Powell's method until the solution is within the boundaries of interest. Finally, algorithm2 presents the algorithm that computes the inverse kinematics implementing Powell's method and the projection algorithm.

B. WORKSPACE FOR EACH ADL

In our customer discovery [5] we conducted 220+ interviews with elderly individuals living at the assisted living centers, individuals with upper and/or lower extremities dysfunctions, educators/researchers working on rehab/assistive robotics, stroke survivors, occupational therapists (OTs), recreational therapists (RTs), physiotherapists (PTs), clinicians, caregivers, family members, wheelchair and assistive device manufacturing companies and distributors, assistive technology professionals (ATPs), and insurance providers to explore pains, market opportunity and trends, and a minimum viable solution to address the needs of the wheelchair-bound individuals with upper extremity dysfunction. Based on the customer discovery 19 essential ADLs are listed for this experiment. ADLs are assessment tools to determine an individual's functional status and the level of care services required to maintain a good quality of life. Throughout the customer discovery the Lawton IADL scale [42] and Bristol activities of daily living scale [43] were used. After exploring

Algorithm 2 Inverse Kinematics

```
procedure InverseKinematics($g, f, \theta, \underline{\theta_i}, \overline{\theta_i}$)
    Tol $\leftarrow$ Tolerance
    MaxIter $\leftarrow$ Maximum Iteration
    Iter $\leftarrow 0$
    while $\theta^* > Tol$ and$Iter < MaxIter$ do
        $\theta \leftarrow Powell(g,\ f,\ \theta)$
        $\theta \leftarrow Projection(\theta,\ \underline{\theta_i},\ \overline{\theta_i})$
        $Iter \leftarrow Iter + 1$
    end while
    return $\theta$
end procedure
```

TABLE 2. Box constraints of each joint of xArm 6 [41]. Values in degree.

Joint	$\underline{\theta_i}$	$\overline{\theta_i}$
Joint 1	−360	360
Joint 2	−118	120
Joint 3	−225	11
Joint 4	−360	360
Joint 5	−97	180
Joint 6	−360	360

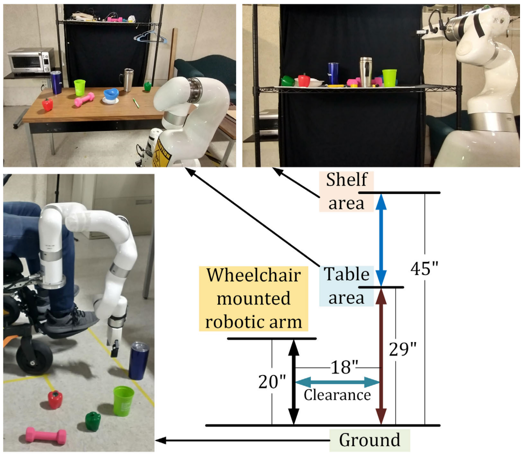

FIGURE 2. Experimental setup to measure workspace of the ADLs.

TABLE 3. Categorization of the listed essential ADLs.

Categories	Essential ADLs
CATEGORY 1	Picking/ Placing objects from table
	Holding spoon/fork
	Maneuvering spoon/fork to take food from bowl to plate
	Holding credit cards, Swipe credit cards at the shop, ATM booth
	Opening/ closing lid of a jar, box, paper box, cap of bottles
	Holding printed books, turning pages
CATEGORY 2	Picking/ Placing objects from ground
CATEGORY 3	Picking/ Placing objects from man reach, upper shelf
CATEGORY 4	Opening closing drawers
CATEGORY 5	Push-pull, Swing open-close doors
	Opening/ closing Refrigerator, Oven
CATEGORY 6	Holding cup near the mouth
	Gradual upward positioning of the cup while drinking
	Maneuvering spoon/fork to take food from bowl to plate
	Maneuvering spoon/fork to put food to the mouth
	Putting pills/medicine in the mouth
	Holding the phone near the ear or put in speaker mode
CATEGORY 7	Holding Pen, Maneuvering on paper or surfaces

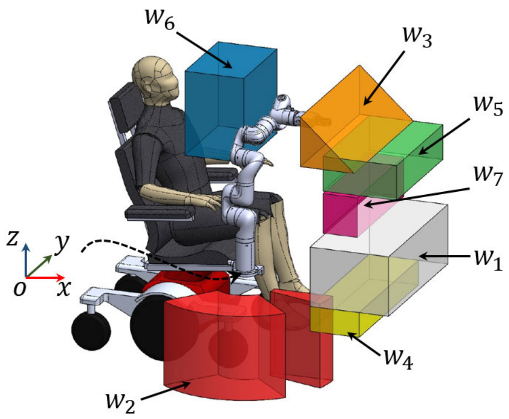

FIGURE 3. Representation of the workspaces of each ADLs relative to the robot and the user.

the positions of the objects associated with the ADLs, we grouped the 19 ADLs, categorizing them into seven different groups. Table 3 presents each category, including the correspondent ADLs. Figure 2 depicts a few of the ADLs experimental setup while measuring the workspace. All ADLs consider a clearance relative to the robot to ensure the collision-free movement of the end-effector. We removed the user's blind spots from the workspace, though the end-effector can cover those areas. Figure 3 represents the measured workspace relative to the wheelchair, and Fig. 4 presents the dimensions of each ADL workspace category, including the end-effector's orientation. Note that the end-effector orientation uses the same orientation of the human hand approaching to manipulate specific objects [44].

C. COLLISION ALGORITHM

The collision algorithm determines if there is a collision between two OBB objects, as described in [25]. An i OBB object is presented in Figure (5a), where $\vec{c}^{\,(i)}$ is the center of the OBB; the three $e_k^{(i)}$ are the half box dimension along the e_k^i direction; the three $u_k^{(i)}$ are three orthonormal vectors that represent the OBB orientation. The three orthonormal vectors form the following rotation matrix:

$$R^{(i)} = \left[\hat{u}_0^{(i)}\ \hat{u}_1^{(i)}\ \hat{u}_2^{(i)}\right] \tag{10}$$

Then, the collision between two OBB is obtained considering figure (5b). In this figure, the distance vector between the center of the two OBB is as follows:

$$\vec{T} = \vec{c}^{\,(j)} - \vec{c}^{\,(i)} \tag{11}$$

The vector $\vec{T}$ is then projected to 15 separating axes. The separating axes are constituted by the vectors of $R^{(i)}$ and $R^{(j)}$ as established in equation (10), and by the cross products:

$$P_k = \left[\hat{u}_k^{(i)} \times \hat{u}_0^{(j)}\ \hat{u}_k^{(i)} \times \hat{u}_1^{(j)}\ \hat{u}_k^{(i)} \times \hat{u}_2^{(j)}\right] \text{ for } k = 0, 1, 2 \tag{12}$$

Thus, the projection of $\vec{T}$ to each separating axes is as follows:

$$T_L = \begin{bmatrix} R^{(i)^t} \\ R^{(j)^t} \\ P_0^t \\ P_1^t \\ P_2^t \end{bmatrix} \vec{T} \tag{13}$$

where the t super-index represents the transpose. Additionally, the projection of each OBB edge to each separating axes

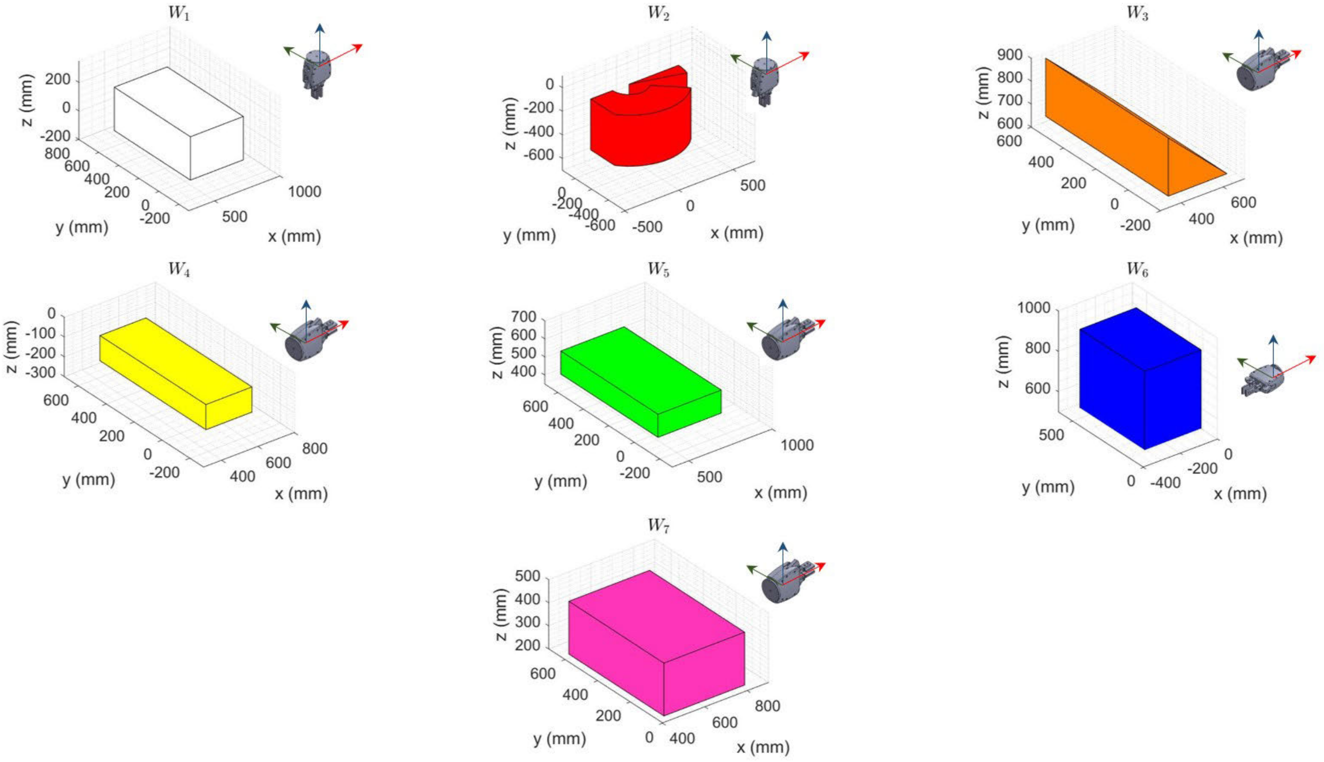

FIGURE 4. Dimensions and location of each ADL workspace, including the orientation of the end-effector relative to *O*.

is as follows:

$$r_L^{(i)} = \begin{bmatrix} I \\ |R^{(j)^t} R^{(i)}| \\ |P_0^t R^{(i)}| \\ |P_1^t R^{(i)}| \\ |P_2^t R^{(i)}| \end{bmatrix} \begin{bmatrix} e_0^{(i)} \\ e_1^{(i)} \\ e_2^{(i)} \end{bmatrix} \tag{14}$$

where I is a 3×3 identity matrix. Then, the following relation is verified to check if the objects are separated:

$$|T_L| > r^{(i)} + r^{(j)} \tag{15}$$

Note that T_L is 15×1 vector. If at least one inequality of equation (15) is satisfied, the boxes are not under collision; otherwise, they are colliding.

The collision algorithm determines the collision between the robot itself and the user. The algorithm that checks for all the possible collisions is *collision checker*, as presented in Algorithm (3). Thus, the algorithm considers every robot link within an OBB or group of OBBs and the user within four OBBs. Figure (6) presents the OBBs that contain the user and the robot. The position and orientation of each OBB are obtained using DH parameters, as shown in Table (4). Note that the values of each $\vec{c}^{\,(i)}$ are measured at the coordinate system resulting from the DH transformations.

Algorithm 3 Collision Checker

```
procedure CollisionChecker
    for $i = 1;\ \ i \le 4;\ \ i++$ do
        for $j = i + 2;\ \ j \le 6;\ \ j++$ do
            if Link $i$ collides with Link $j$ then    ▷ Check collision between the robot with itself
                return True
            end if
        end for
    end for
    for $i = 1;\ \ i \le 6;\ \ i++$ do
        for $j = 1;\ \ j \le 4;\ \ j++$ do
            if Link $i$ collides with User box $j$ then    ▷ Check collision between the robot with the user
                return True
            end if
        end for
    end for
    return False
end procedure
```

D. SINGULARITY ANALYSIS

Manipulability is the capacity of a robot to maneuver within a workspace [45]. Many strategies compute the manipulability

TABLE 4. DH parameters, centers, and dimensions of each OBB.

	Link	Box	a	α	d	θ	$c_x^{(i)}$	$c_y^{(i)}$	$c_z^{(i)}$	$e_0^{(i)}$	$e_1^{(i)}$	$e_2^{(i)}$
Robot	Link 1	r_0	0	0	155	0	0	0	-77.50	47.50	47.50	77.50
		r_1	0	0	112	θ_1	0	0	-56.00	95.00	47.50	79.75
	Link 2	r_2	0	-$\pi/2$	0	θ_2	0	82.50	-54.50	95.00	47.50	102.00
			0	$\pi/2$	109	0						
		r_3	0	-$\pi/2$	0	β_1	-91.50	0	0	115.25	47.50	47.50
			183.00	0	0	0						
	Link 3	r_4	0	0	0	θ_3+β_2	-57.05	0	82.50	104.55	47.50	47.50
			114.10	0	0	0						
		r_5	0	0	0	β_3	-66.45	0	0	66.45	47.50	47.50
			85.40	0	0	0						
	Link 4	r_6	0	0	0	-$\pi/2$	0	0	1.39	46.11	47.50	47.50
			0	-$\pi/2$	45	θ_4						
		r_7	0	0	128	0	0	82.50	-64.14	47.50	35.00	111.64
	Link 5	r_8	0	$\pi/2$	0	θ_5	-38.00	0	0	85.50	47.50	47.50
			76.00	0	0	0						
	Link 6 + Gripper	r_9	0	-$\pi/2$	275	θ_6	0	0	-113.65	47.50	47.50	113.65
Chair	User box 1	c_1	0	0	0	0	-457.2	330.2	-355.6	457.2	165.1	342.9
	User box 2	c_2	0	0	0	0	-165.1	165.1	12.7	177.8	215.9	342.9
	User box 3	c_3	0	0	0	0	-558.8	342.9	641.4	228.6	266.7	419.1
	User box 4	c_4	0	0	0	0	88.9	355.6	-127.0	177.0	381.0	203.2

of a robot by considering the product of the eigenvalues or the determinant of the jacobian matrix and using them to find the singular configurations of the robot [46], [47], [48], [49]. However, these manipulability measures come with multiple issues. For example, the eigenvalues of the jacobian matrix may be inconsistent because the kinematics of the manipulator depends on the position and orientation of the end-effector [50]. Thus, the manipulability index is suitable to compute on cartesian robots of 3-DOF [51] or in robots with positions independent of the orientation like PUMA [52], [53]. To solve this issue, Kim et al. proposed a methodology for standardizing the units of the Jacobian matrix by homogenizing the eigenvalues [54]. However, this method assumes an arbitrary length for the standard jacobian matrix; since it can take any value, it may hide errors in the manipulator position [55], [56]. Thus, this research considers two manipulability measures: one for the end-effector displacement and another for rotation. Two different manipulability measures imply two different Jacobian matrices, which are derived as follows:

$$J_t = \begin{bmatrix} \frac{\delta\, {}^0P_6}{\delta\theta_1} & \frac{\delta\, {}^0P_6}{\delta\theta_2} & \frac{\delta\, {}^0P_6}{\delta\theta_3} & \frac{\delta\, {}^0P_6}{\delta\theta_4} & \frac{\delta\, {}^0P_6}{\delta\theta_5} & \frac{\delta\, {}^0P_6}{\delta\theta_6} \end{bmatrix}$$
$$J_\theta = \begin{bmatrix} J_{\theta_x} \\ J_{\theta_y} \\ J_{\theta_z} \end{bmatrix} \qquad (16)$$

where J_t and J_θ are the translational and rotational Jacobian matrices, respectively. The sub-matrices J_{θ_x}, J_{θ_y}, and J_{θ_z} are as follows:

$$J_{\theta_x} = \begin{bmatrix} {}^0R_6(3,1) & {}^0R_6(3,2) & {}^0R_6(3,3) \end{bmatrix} \begin{bmatrix} \frac{\partial\, {}^0R_6^T}{\partial\theta}(2,1) \\ \frac{\partial\, {}^0R_6^T}{\partial\theta}(2,2) \\ \frac{\partial\, {}^0R_6^T}{\partial\theta}(2,3) \end{bmatrix}$$

$$J_{\theta_y} = \begin{bmatrix} {}^0R_6(1,1) & {}^0R_6(1,2) & {}^0R_6(1,3) \end{bmatrix} \begin{bmatrix} \frac{\partial\, {}^0R_6^T}{\partial\theta}(3,1) \\ \frac{\partial\, {}^0R_6^T}{\partial\theta}(3,2) \\ \frac{\partial\, {}^0R_6^T}{\partial\theta}(3,3) \end{bmatrix}$$

$$J_{\theta_z} = \begin{bmatrix} {}^0R_6(2,1) & {}^0R_6(2,2) & {}^0R_6(2,3) \end{bmatrix} \begin{bmatrix} \frac{\partial\, {}^0R_6^T}{\partial\theta}(1,1) \\ \frac{\partial\, {}^0R_6^T}{\partial\theta}(1,2) \\ \frac{\partial\, {}^0R_6^T}{\partial\theta}(1,3) \end{bmatrix}$$

Then, using the results from Equation (16), the two manipulability measures are as follows:

$$\mathcal{M}_t = \frac{|\underline{\sigma}_t|}{|\overline{\sigma}_t|}$$

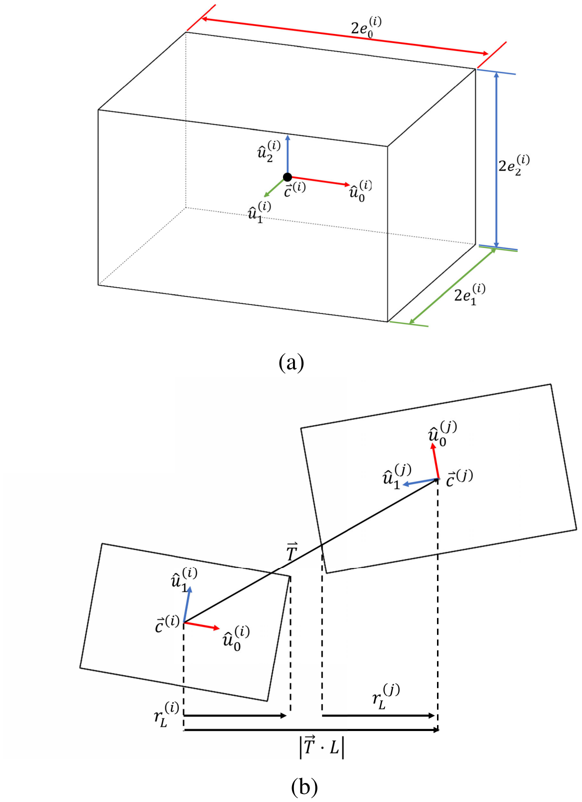

(a)

(b)

FIGURE 5. (a) OBB representation, (b) The distance between two OBBs is less than the total of their projected radii for some axis L.

Algorithm 4 Manipulability Checker

```
procedure ManipulabilityChecker($\mathcal{M}_t$, $\mathcal{M}_\theta$)
    if $\mathcal{M}_t > 0$ and$\mathcal{M}_\theta > 0$ then
        return True
    end if
    return False
end procedure
```

$$\mathcal{M}_\theta = \frac{|\underline{\sigma}_\theta|}{|\overline{\sigma}_\theta|} \tag{17}$$

where $\overline{\sigma}$ and $\underline{\sigma}$ are the maximum eigenvalues of the matrix JJ^t. The *manipulability checker* algorithm is presented in algorithm 4.

E. OBJECTIVE FUNCTION

The objective is to find the base location that maximizes the workspace available for the robot. To this end, each pose within the workspaces defined in section (II-B) must satisfy the following constraints:

- Inverse kinematic solution within the joint limits, as determined by Equation (9).
- No collision, as determined by the *collision checker*.
- No singularities, as determined by the *Manipulability checker*.

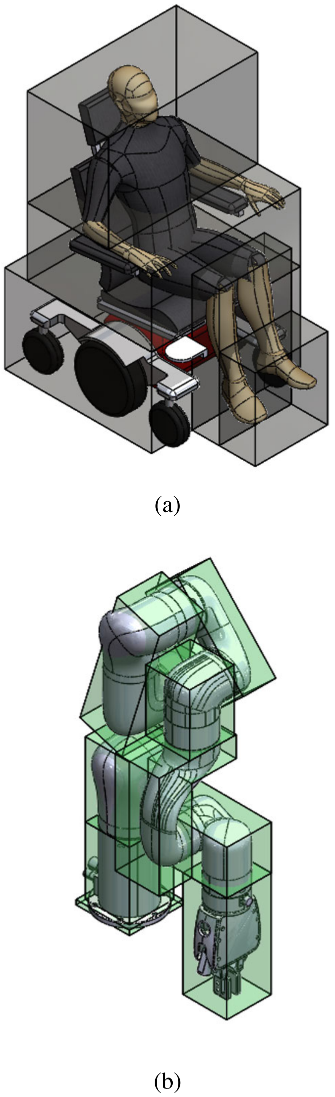

(a)

(b)

FIGURE 6. (a) The user is within three OBBs, and (b) Each link of the robot is within an OBB or a group of OBBs.

Thus, consider $\mathcal{W}$ as the sum of the individual workspaces (w_i), such that:

$$\mathcal{W} = w_1 \cup w_2 \cup \cdots \cup w_n \tag{18}$$

Then, letting P_i be an i goal pose within $\mathcal{W}$ that satisfies the mentioned constraints, the objective function is as follows:

$$F(N, P_b) = \frac{\sum_i^{N_s} P_i}{N} \times 100 \tag{19}$$

where N represents all the points of $\mathcal{W}$ after discretization, with N_s being a subset of N with all the reachable points. P_b is the new position of the base location. Thus, equation (19) is the percentage of workspace coverage.

Note that the new base location P_b is related to the initial orientation of the robot by using the HTM ${}^bT_0$, as defined

Algorithm 5 Objective Function

```
procedure ObjectiveFunction($N$, $P_b$, f, $\theta$, $\underline{\theta}$, $\overline{\theta}$)
    ${}^{b}T_6 \leftarrow {}^{b}T_0\,{}^{0}T_6$
    $f(\theta) \leftarrow Pose({}^{b}T_6)$
    $N_s \leftarrow 0$
    Tol ← Tolerance
    for $P_i$ in $\mathcal{W}$ do
        $\theta \leftarrow InverseKinematics(P_i,\ f(\theta),\ \theta,\ \underline{\theta},\ \overline{\theta})$
        $\theta^* = \frac{1}{2}\|P_i - f(\theta)\|$
        if $\theta^* < Tol$ then
            if not CollisionChecker then
                if ManipulabilityChecher then
                    $N_s \leftarrow N_s + 1$
                end if
            end if
        end if
    end for
    return $\frac{N_s}{N} \times 100$
end procedure
```

below:

$$
{}^{b}T_0 = \begin{bmatrix} 1 & 0 & 0 & P_{bx} \\ 0 & 1 & 0 & P_{by} \\ 0 & 0 & 1 & P_{bz} \\ 0 & 0 & 0 & 1 \end{bmatrix} \tag{20}
$$

This HTM modifies the initial base by multiplying the HTM of equation (5) as follows:

$$
{}^{b}T_6 = {}^{b}T_0\,{}^{0}T_6 \tag{21}
$$

where ${}^{b}T_6$ is the end-effector position after moving the base from the initial position. Thus, the new ${}^{b}T_6$ is used to define f as $f(\theta) = Pose({}^{b}T_6)$, this result is then used in equation (9) and in algorithm 2 to compute the inverse kinematics. Finally, algorithm 5 presents the steps to calculate the objective function.

III. OPTIMIZATION METHODOLOGY

This research uses GA for base placement optimization, the most common strategy available in the literature for base placement optimization. To name a few pieces of research that use this strategy, consider the works of Mitsi et al. They used a hybrid (GA) to find the optimal robot base location considering discrete end-effector positions [57]. Also, Chen and Tseng [58] used GAs to determine the location of the workpiece that satisfies the shortest path requirement between work points that needed to be visited by the robot. Other research uses GA for workspace optimization in the context of kinematics, as is the case of Zhao et al. [59]. GA has the advantage that it can escape from local optimums, making it a powerful global search method [60]. Thus, Algorithm (6) presents the GA as presented in [61]. For details on implementing the GA, the reader is encouraged to read [61].

Algorithm 6 Genetic Algorithm

```
procedure GeneticAlgorithm(Population size ($\mathcal{P}$), Generations ($\mathcal{G}$), Optimization limits)
    Create an initial population.
    Evaluate the objective function for each member of the initial population.
    for $i = 1;\ \ i \leq \mathcal{G};\ \ i++$ do
        Create a new population using crossover and mutation functions.
        Calculate the objective function for each member of the new population.
        Merge all the population members with the new population.
        From the merged population, select the fittest members for the next generation.
    end for
    return Best member of the last generation.
end procedure
```

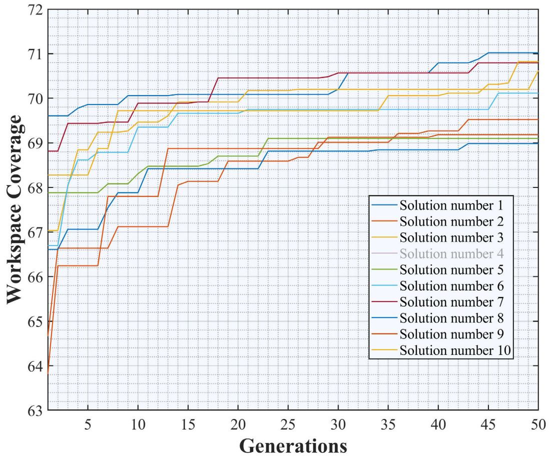

FIGURE 7. The results of the optimization for different random initial values.

TABLE 5. Parameters for the genetic algorithm. The limit values are in *mm*.

Parameters	Values
$\mathcal{P}$	12
$\mathcal{G}$	50
x_{limits}	[0, 254]
y_{limits}	[-127, 50.8]
z_{limits}	[-127, 127]

TABLE 6. Optimal base position relative to $\mathcal{O}$.

x (mm)	y (mm)	z (mm)
205	50	86

IV. RESULTS

The GA is implemented to find the optimal base placement using the parameters presented in Table (5). $\mathcal{P}$ and $\mathcal{G}$ were

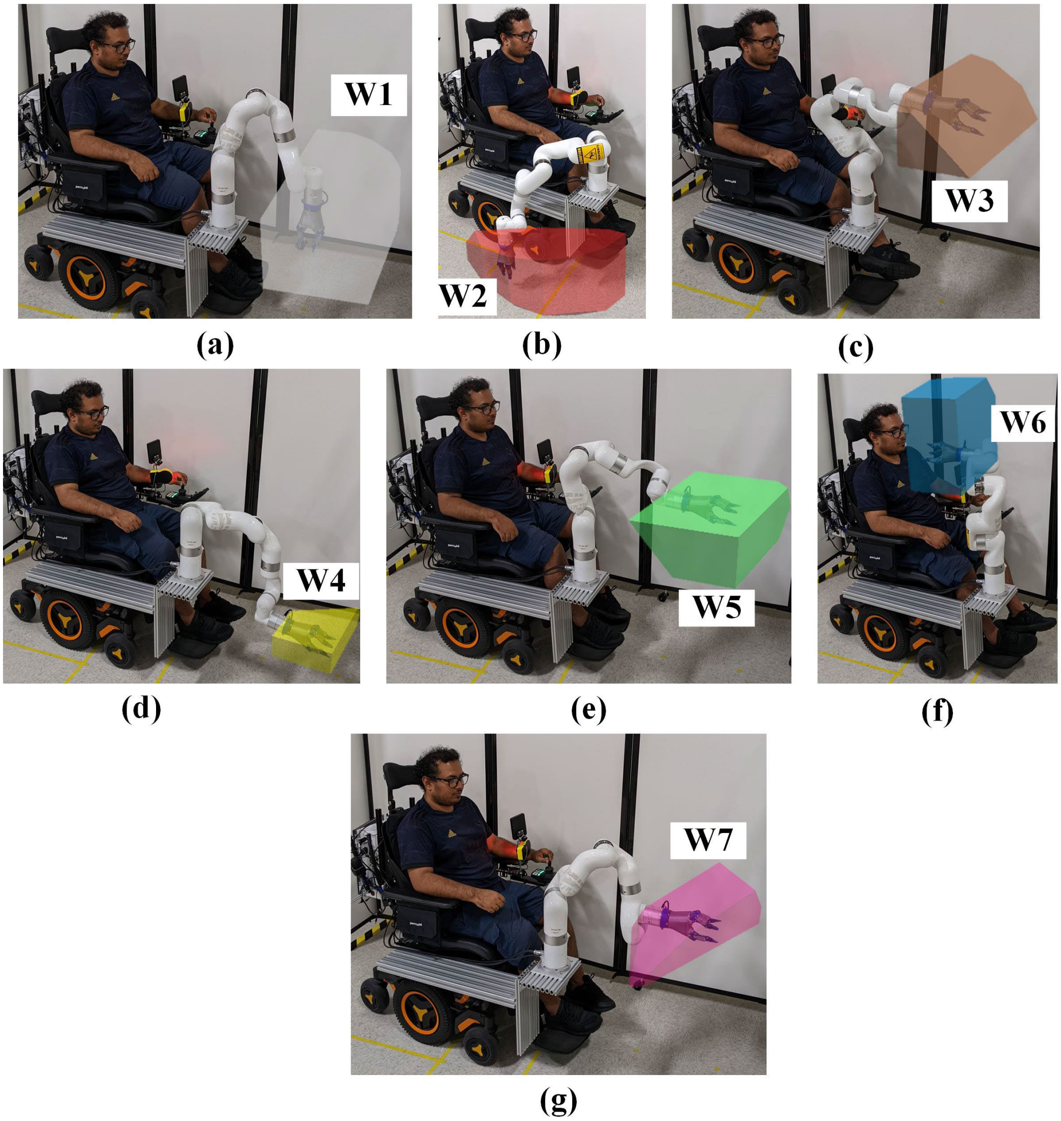

FIGURE 8. Experimental validation of the workspace coverage of the robot with the optimal base placement.

TABLE 7. Comparison of Workspace Coverage for the original and the optimized base position.

	Workspace Coverage		
Category	Origin	Optimized	Validation
W1	32%	93%	93%
W2	72%	63%	64%
W3	17%	85%	86%
W4	20%	23%	25%
W5	11%	84%	87%
W6	9%	90%	91%
W7	10%	12%	14%
Total	25%	69%	71%

selected to minimize the computation time. The optimization limits (the region of exploration to find the optimum) were selected considering two criteria the location of the patient and the tilting moment generated by the robot. Ten base placement optimizations were conducted from different random initial values. Figure (7) presents the results of the optimizations. Table (6) shows the best solution obtained from the ten optimizations. Figure (8) the new base build for workspace validation. For the validation, we explored the points within the robot workspace to produce the shapes presented in Figure (8). Table (7) compares the percentage of workspace coverage for the robot at the optimal base, the experiment, and at the initial position ($\mathcal{O}$). Note that the workspace coverage increased from a 25% to 71%. Also, note that the workspace generated by the validation is bigger than the workspace generated by the optimization. This difference happens because the OBBs are still a conservative way of representing the shape of the links or the patient. Although the GA optimization may require a more rigorous implementation, the results indicate the capabilities of the methodology presented in the article, which yielded a base placement that increased the workspace almost three times the initial value, with a workspace free of collisions and singularities.

V. CONCLUSION

This article presents an objective function for the base placement optimization of an assistive robot attached to a wheelchair. For this purpose, we defined the workspace coverage of the robot to fulfill a list of ADLs. Then, the proposed method uses an object collision algorithm that determines the collision between the user and the robot using OBBs to describe the robot links, the user, and the wheelchair. Also, the proposed methodology divides the jacobian matrix into two parts. One part is the jacobian that transforms the joint velocities into end-effector velocities, while the other does for the end-effector angular velocities. This way, we avoid inconsistencies in calculating the relationship between the eigenvalues of the jacobian matrix, which determine the singularities for the position and orientation of the robot. Then, the proposed method removes the points within the workspace if a collision or singularities are detected. Thus, we defined the workspace coverage as the percentage of the desired workspace without collisions and singularities, with the workspace coverage as our objective function for optimization. Then, using a GA, we searched for the optimal base that maximizes the objective function obtaining a new base placement with a workspace coverage almost three times the workspace coverage at the initial position. The workspace coverage was validated experimentally by exploring the workspace using the xArm robot.

ACKNOWLEDGMENT

The contents of this research do not necessarily represent the policy of NIDILRR, ACL, or HHS, and they should not assume endorsement by the Federal Government.

REFERENCES

[1] Reeve Foundation. *Stats About Paralysis*. Accessed: Aug. 1, 2020. [Online]. Available: https://www.christopherreeve.org/living-with-paralysis/stats-about-paralysis

[2] (Oct. 2022). *Family Caregivers Provide $470 Billion in Unpaid Care as Role Becomes More Complicated*. Accessed: Oct. 7, 2022. [Online]. Available: https://press.aarp.org/2019-11-14-Valuingthe-Invaluable-Series

[3] E. Munoz, M. S. H. Sunny, I. Rulik, J. D. S. De Caro, and M. H. Rahman, "Kinematics and workspace analysis of xArm6 robot for activities of daily living," in *Proc. Int. Conf. Ind. Mech. Eng. Oper. Manag.*, 2021, vol. 4, no. 4, p. 885. [Online]. Available: https://www.ncbi.nlm.nih.gov/pmc/articles/PMC9201617

[4] M. Zahabi, X. Zheng, A. Maredia, and F. Shahini, "Design of navigation applications for people with disabilities: A review of literature and guideline formulation," *Int. J. Hum.-Comput. Interact.*, vol. 2022, pp. 1–23, Jul. 2022.

[5] M. H. Rahman, "NSF I-corps, Customer discovery: Wheelchair mounted robotic assistive arm," Tech. Rep. 1848912, May 2018.

[6] (Oct. 2021). *Breadcrumb*. Accessed: Oct. 7, 2022. [Online]. Available: https://now.aapmr.org/wheelchair-and-power-mobility

[7] (2021). *Meet Obi*. [Online]. Available: https://meetobi.com/

[8] Kinova Inc. (2021). *Kinova Jaco Assistive Robotic Arm*. [Online]. Available: https://www.kinovarobotics.com/en/assistive-technologies/column-a1/kinova-assistive-robotic-arm

[9] M. Iskandar, G. Quere, A. Hagengruber, A. Dietrich, and J. Vogel, "Employing whole-body control in assistive robotics," in *Proc. IEEE/RSJ Int. Conf. Intell. Robots Syst. (IROS)*, Nov. 2019, pp. 5643–5650.

[10] F. Lewis, S. Jagannathan, and A. Yesildirak, *Neural Network Control of Robot Manipulators and Non-Linear Systems*. Boca Raton, FL, USA: CRC Press, 2020.

[11] J. Wang and M. Q.-H. Meng, "Optimal path planning using generalized Voronoi graph and multiple potential functions," *IEEE Trans. Ind. Electron.*, vol. 67, no. 12, pp. 10621–10630, Dec. 2020.

[12] N. C. N. Doan and W. Lin, "Optimal robot placement with consideration of redundancy problem for wrist-partitioned 6R articulated robots," *Robot. Comput.-Integr. Manuf.*, vol. 48, pp. 233–242, Dec. 2017.

[13] M. M. Coad, *Design, Modeling, and Control of Vine Robots for Exploration of Unknown Environments*. Stanford, CA, USA: Stanford Univ., 2021.

[14] M. N. Janardhanan, Z. Li, G. Bocewicz, Z. Banaszak, and P. Nielsen, "Metaheuristic algorithms for balancing robotic assembly lines with sequence-dependent robot setup times," *Appl. Math. Model.*, vol. 65, pp. 256–270, Jan. 2019.

[15] C. Yang, W. Ye, and Q. Li, "Review of the performance optimization of parallel manipulators," *Mechanism Mach. Theory*, vol. 170, Apr. 2022, Art. no. 104725.

[16] Y. Zhou, C.-Y. Chen, G. Yang, and Y. Li, "A sampling-based motion assignment strategy with multi-performance optimization for macro-micro robotic system," *IEEE Robot. Autom. Lett.*, vol. 7, no. 4, pp. 11649–11656, Oct. 2022.

[17] Y. Zhang, S. Li, and X. Zhou, "Recurrent-neural-network-based velocity-level redundancy resolution for manipulators subject to a joint acceleration limit," *IEEE Trans. Ind. Electron.*, vol. 66, no. 5, pp. 3573–3582, May 2019.

[18] M. Elsisi, K. Mahmoud, M. Lehtonen, and M. M. F. Darwish, "An improved neural network algorithm to efficiently track various trajectories of robot manipulator arms," *IEEE Access*, vol. 9, pp. 11911–11920, 2021.

[19] S. Zeghloul and J. A. Pamanes-Garcia, "Multi-criteria optimal placement of robots in constrained environments," *Robotica*, vol. 11, no. 2, pp. 105–110, Mar. 1993.

[20] G. J. A. Pamanes and S. Zeghloul, "Optimal placement of robotic manipulators using multiple kinematic criteria," in *Proc. IEEE Int. Conf. Robot. Autom.*, Jan. 1991, pp. 933–934.

[21] J. A. Pamanes, S. Zeghloul, and J. P. Lallemand, "On the optimal placement and task compatibility of manipulators," in *Proc. 5th Int. Conf. Adv. Robot. Robots Unstructured Environ.*, 1991, pp. 1694–1697.

[22] R. Ur-Rehman, S. Caro, D. Chablat, and P. Wenger, "Path placement optimization of manipulators based on energy consumption: Application to the orthoglide 3-axis," *Trans. Can. Soc. Mech. Eng.*, vol. 33, no. 3, pp. 523–541, Sep. 2009.

[23] D. Spensieri, J. S. Carlson, R. Bohlin, J. Kressin, and J. Shi, "Optimal robot placement for tasks execution," *Proc. CIRP*, vol. 44, pp. 395–400, Jan. 2016.

[24] R. K. Malhan, A. M. Kabir, B. Shah, and S. K. Gupta, "Identifying feasible workpiece placement with respect to redundant manipulator for complex manufacturing tasks," in *Proc. Int. Conf. Robot. Autom. (ICRA)*, May 2019, pp. 5585–5591.

[25] C. Ericson, *Real-Time Collision Detection*. Boca Raton, FL, USA: CRC Press, 2004.

[26] A. Zeiaee, R. Soltani-Zarrin, R. Langari, and R. Tafreshi, "Kinematic design optimization of an eight degree-of-freedom upper-limb exoskeleton," *Robotica*, vol. 37, no. 12, pp. 2073–2086, Dec. 2019.

[27] E. G. López, W. Yu, and X. Li, "Optimum design of a parallel robot using neuro-genetic algorithm," *J. Mech. Sci. Technol.*, vol. 35, no. 1, pp. 293–305, Jan. 2021.

[28] G. Huang, S. Guo, D. Zhang, H. Qu, and H. Tang, "Kinematic analysis and multi-objective optimization of a new reconfigurable parallel mechanism with high stiffness," *Robotica*, vol. 36, no. 2, pp. 187–203, Feb. 2018.

[29] J.-A. Leal-Naranjo, M. Ceccarelli, C.-R. Torres-San-Miguel, L.-A. Aguilar-Perez, G. Urriolagoitia-Sosa, and G. Urriolagoitia-Calderón, "Multi-objective optimization of a parallel manipulator for the design of a prosthetic arm using genetic algorithms," *Latin Amer. J. Solids Struct.*, vol. 15, no. 3, pp. 1–15, May 2018.

[30] M. H. Rahman, T. Kittel-Ouimet, M. Saad, J.-P. Kenné, and P. S. Archambault, "Dynamic modeling and evaluation of a robotic exoskeleton for upper-limb rehabilitation," *Int. J. Inf. Acquisition*, vol. 8, no. 1, pp. 83–102, Mar. 2011.

[31] R. Zhao, Z. Shi, Y. Guan, Z. Shao, Q. Zhang, and G. Wang, "Inverse kinematic solution of 6R robot manipulators based on screw theory and the Paden–Kahan subproblem," *Int. J. Adv. Robot. Syst.*, vol. 15, no. 6, 2018, Art. no. 1729881418818297.

[32] J. S. De Caro, M. R. Islam, E. M. Montenegro, B. Brahmi, and M. Rahman, "Inverse kinematic solution of u-Rob4 an hybrid exoskeleton for stroke rehabilitation," in *Proc. 18th Int. Multi-Conf. Syst., Signals Devices (SSD)*, Mar. 2021, pp. 755–764.

[33] C. Lauretti, T. Grasso, E. de Marchi, S. Grazioso, and G. di Gironimo, "A geometric approach to inverse kinematics of hyper-redundant manipulators for tokamaks maintenance," *Mechanism Mach. Theory*, vol. 176, Oct. 2022, Art. no. 104967.

[34] G. Fang, C.-D. Matte, R. B. N. Scharff, T.-H. Kwok, and C. C. L. Wang, "Kinematics of soft robots by geometric computing," *IEEE Trans. Robot.*, vol. 36, no. 4, pp. 1272–1286, Aug. 2020.

[35] V. I. Petrenko, F. B. Tebueva, M. M. Gyrchinsky, V. O. Antonov, and J. A. Shutova, "The method of forming a geometric solution of the inverse kinematics problem for chains with kinematic pairs of rotational type only," *IOP Conf. Ser., Mater. Sci. Eng.*, vol. 450, Nov. 2018, Art. no. 042016.

[36] J. Guzmán-Giménez, Á. V. Fernández, V. M. Amela, and M. Á. Díaz-Rodríguez, "Synthesis of the inverse kinematic model of non-redundant open-chain robotic systems using Groebner basis theory," *Appl. Sci.*, vol. 10, no. 8, p. 2781, Apr. 2020.

[37] A. Aristidou, J. Lasenby, Y. Chrysanthou, and A. Shamir, "Inverse kinematics techniques in computer graphics: A survey," *Comput. Graph. Forum*, vol. 37, no. 6, pp. 35–58, Sep. 2018.

[38] S.-O. Park, M. C. Lee, and J. Kim, "Trajectory planning with collision avoidance for redundant robots using Jacobian and artificial potential field-based real-time inverse kinematics," *Int. J. Control, Autom. Syst.*, vol. 18, no. 8, pp. 2095–2107, Aug. 2020.

[39] L. Unzueta, M. Peinado, R. Boulic, and Á. Suescun, "Full-body performance animation with sequential inverse kinematics," *Graph. Models*, vol. 70, no. 5, pp. 87–104, Sep. 2008.

[40] J. J. Moré, B. S. Garbow, and K. E. Hillstrom, "User guide for MINPACK-1," Argonne Nat. Lab., Argonne, IL, USA, Tech. Rep. ANL-80-74, 1980.

[41] Ufactory. (2021). *Xarm Product Page*. [Online]. Available: https://www.ufactory.cc/pages/xarm-product-page

[42] E. I. Isik, S. Yilmaz, I. Uysal, and S. Basar, "Adaptation of the Lawton instrumental activities of daily living scale to Turkish: Validity and reliability study," *Ann. Geriatric Med. Res.*, vol. 24, no. 1, p. 35, 2020.

[43] W. A. Alkeridy, T. A. Muayqil, R. A. Al Khalifah, A. S. Mohammedin, R. A. Khallaf, and R. S. Bucks, "Arabic translation and cross-cultural adaptation of the Bristol activities of daily living scale (BADLS)," *Alzheimer's Dementia*, vol. 17, no. S8, Dec. 2021, Art. no. e050856.

[44] A. M. Dollar, "Classifying human hand use and the activities of daily living," in *The Human Hand as an Inspiration for Robot Hand Development*. Cham, Switzerland: Springer, 2014, pp. 201–216.

[45] S. Pedrammehr, M. R. C. Qazani, H. Asadi, and S. Nahavandi, "Kinematic manipulability analysis of hexarot simulators," in *Proc. IEEE Int. Conf. Ind. Technol. (ICIT)*, Feb. 2019, pp. 133–138.

[46] G. Li, L. Cheng, and N. Sun, "Design, manipulability analysis and optimization of an index finger exoskeleton for stroke rehabilitation," *Mechanism Mach. Theory*, vol. 167, Jan. 2022, Art. no. 104526.

[47] A. Torabi, M. Khadem, K. Zareinia, G. R. Sutherland, and M. Tavakoli, "Manipulability of teleoperated surgical robots with application in design of master/slave manipulators," in *Proc. Int. Symp. Med. Robot. (ISMR)*, Mar. 2018, pp. 1–6.

[48] C. Valsamos, V. Moulianitis, and N. Aspragathos, "Index based optimal anatomy of a metamorphic manipulator for a given task," *Robot. Comput.-Integr. Manuf.*, vol. 28, no. 4, pp. 517–529, Aug. 2012.

[49] J. Eden, D. Lau, Y. Tan, and D. Oetomo, "Unilateral manipulability quality indices: Generalized manipulability measures for unilaterally actuated robots," *J. Mech. Des.*, vol. 141, no. 9, Sep. 2019, pp. 1–13.

[50] Y. Wang, B. Belzile, J. Angeles, and Q. Li, "Kinematic analysis and optimum design of a novel 2PUR–2RPU parallel robot," *Mechanism Mach. Theory*, vol. 139, pp. 407–423, Sep. 2019.

[51] H. Shen, Y.-J. Pan, and G. Bauer, "Manipulability-based load allocation and kinematic decoupling in cooperative manipulations," in *Proc. IEEE 28th Int. Symp. Ind. Electron. (ISIE)*, Jun. 2019, pp. 1168–1173.

[52] P. S. Shiakolas, D. Koladiya, and J. Kebrle, "Optimum robot design based on task specifications using evolutionary techniques and kinematic, dynamic, and structural constraints," *Inverse Problems Eng.*, vol. 10, no. 4, pp. 359–375, 2002.

[53] M. Ceccarelli, G. Carbone, and E. Ottaviano, "An optimization problem approach for designing both serial and parallel manipulators," in *Proc. Int. Sym. Multibody Syst. Mechatronics*, 2005, pp. 6–9.

[54] Y. Li, X. Yang, H. Wu, and B. Chen, "Optimal design of a six-axis vibration isolator via Stewart platform by using homogeneous Jacobian matrix formulation based on dual quaternions," *J. Mech. Sci. Technol.*, vol. 32, no. 1, pp. 11–19, Jan. 2018.

[55] J. P. Merlet, "Jacobian, manipulability, condition number, and accuracy of parallel robots," *J. Mech. Des.*, vol. 128, no. 1, pp. 199–206, Jan. 2006.

[56] F. Vidussi, P. Boscariol, L. Scalera, and A. Gasparetto, "Local and trajectory-based indexes for task-related energetic performance optimization of robotic manipulators," *J. Mech. Robot.*, vol. 13, no. 2, pp. 1–15, Apr. 2021.

[57] S. Mitsi, K.-D. Bouzakis, D. Sagris, and G. Mansour, "Determination of optimum robot base location considering discrete end-effector positions by means of hybrid genetic algorithm," *Robot. Comput.-Integr. Manuf.*, vol. 24, no. 1, pp. 50–59, Feb. 2008.

[58] C.-J. Chen and C.-S. Tseng, "The path and location planning of workpieces by genetic algorithms," *J. Intell. Manuf.*, vol. 7, no. 1, pp. 69–76, Feb. 1996.

[59] J. Zhao, C. Wu, G. Yang, C.-Y. Chen, S. Chen, C. Xiong, and C. Zhang, "Kinematics analysis and workspace optimization for a 4-DOF 3T1R parallel manipulator," *Mechanism Mach. Theory*, vol. 167, Jan. 2022, Art. no. 104484.

[60] Y. Su, Y. Qiu, P. Liu, J. Tian, Q. Wang, and X. Wang, "Dynamic modeling, workspace analysis and multi-objective structural optimization of the large-span high-speed cable-driven parallel camera robot," *Machines*, vol. 10, no. 7, p. 565, Jul. 2022.

[61] M. Gen and R. Cheng, *Genetic Algorithms and Engineering Optimization*, vol. 7. Hoboken, NJ, USA: Wiley, 1999.

JAVIER DARIO SANJUAN DE CARO received the B.S. and M.S. degrees in mechanical engineering from the Universidad del Norte, Colombia, in 2013 and 2016, respectively. He is currently pursuing the Ph.D. degree with the Biorobotics Laboratory, University of Wisconsin–Milwaukee. His research interests include dynamics, control, and inverse kinematics. He has served as an Invited Reviewer for *Mechanisms and Machine Theory* journal, IEEE Latin America Transactions, and other scientific publications. Besides, he is one of the founders of the Vertical Integrated Projects (VIP) Student Association with the Universidad del Norte.

MD. SAMIUL HAQUE SUNNY was born in Netrokona, Bangladesh, in 1994. He received the B.S. degree in electrical and electronic engineering from the Khulna University of Engineering and Technology, in 2017. He is currently pursuing the Ph.D. degree with the Biorobotics Laboratory, University of Wisconsin–Milwaukee, with a background in artificial intelligence, digital signal and image processing, data mining, robotics, biological signal processing, human–machine interface design, and power system stability. He is also developing an eye-gaze-controlled user interface deployable to Hololnes-2's mixed-reality platform to enable a collaborative work environment for individuals with limited upper limb movement, EEG signal for better BCI application, and structures of CNN for upgrading its performance in image recognition.

ELIAS JOSE MUÑOZ MONTENEGRO received the bachelor's degree in mechanical engineering from the Universidad del Norte, Colombia, in 2019. He is currently pursuing the M.S. degree with the Biorobotics Laboratory, University of Wisconsin–Milwaukee. More than five years, he has been researching mechatronics/robotics with emphasis on the analysis and simulation of serial and parallel robot.

HELAL UDDIN AHMED received the B.Sc. degree in engineering (mechanical) from the Khulna University of Engineering and Technology, Bangladesh, in 2001, and the M.E. degree from the Bangladesh University of Engineering and Technology, Bangladesh, in 2004. He is currently a Research Collaborator with the Biorobotics Laboratory, Mechanical Engineering Department, University of Wisconsin–Milwaukee, Milwaukee, WI, USA. He has been the Deputy General Manager (Validation) of the Engineering Department, Toray Industries Ltd., (TMBD, Bangladesh), since 2010.

MOHAMMAD H. RAHMAN (Senior Member, IEEE) received the B.Sc. degree in engineering (mechanical) from the Khulna University of Engineering and Technology, Bangladesh, in 2001, the M.E. degree in biorobotics from Saga University, Japan, in 2005, and the Ph.D. degree in engineering (bio-robotics) from the École de technologie supérieure (ETS), Université du Québec, Canada, in 2012. He worked as a Postdoctoral Research Fellow with the School of Physical and Occupational Therapy, McGill University, from 2012 to 2014. He is currently a Richard and Joanne Grigg Professor and an Associate Professor in biomedical engineering and mechanical engineering at the University of Wisconsin–Milwaukee, Milwaukee, WI, USA. As the Director of the Biorobotics Laboratory, University of Wisconsin–Milwaukee, he brings the resources and expertise of an interdisciplinary research and development team. For more than 15 years, he has been researching bio-mechatronics/bio-robotics with emphasis on the design, development, and control of wearable robots to rehabilitate and assist elderly and physically disabled individuals, who have lost their upper-limb function or motion due to stroke, cardiovascular disease, trauma, sports injuries, occupational injuries, and spinal cord injuries. His research interests include bio-robotics, exoskeleton robots, intelligent systems and control, mobile robotics, nonlinear control, and control using biological signals, such as electromyogram signals.